Journal of Membrane Science and Research 6 (2020) 333-343

Journal of Membrane Science & Research

journal homepage: www.msrjournal.com

Research Paper

Selective Mass Transport of CO_2 Containing Mixtures through Zeolite Membranes

Pasquale Francesco Zito, Adele Brunetti *, Giuseppe Barbieri

National Research Council – Institute on Membrane Technology (ITM-CNR), Via Pietro BUCCI, Cubo 17C, 87036 Rende CS, Italy

Article info

Received 2020-04-08
Revised 2020-06-01
Accepted 2020-06-03
Available online 2020-06-03

Keywords

Gas separation
Maxwell-Stefan
CO_2 capture
CH_4 purification

Highlights

- Zeolite membranes for selective separation of CO_2 from H_2, CH_4 and N_2
- Mass transport through zeolite membranes described by surface diffusion competing with gas translation diffusion
- Analysis of the effect exerted by temperature and driving force on permeance and selectivity
- Permeance and selectivity of CO_2 higher in mixture than in single gas

Graphical abstract

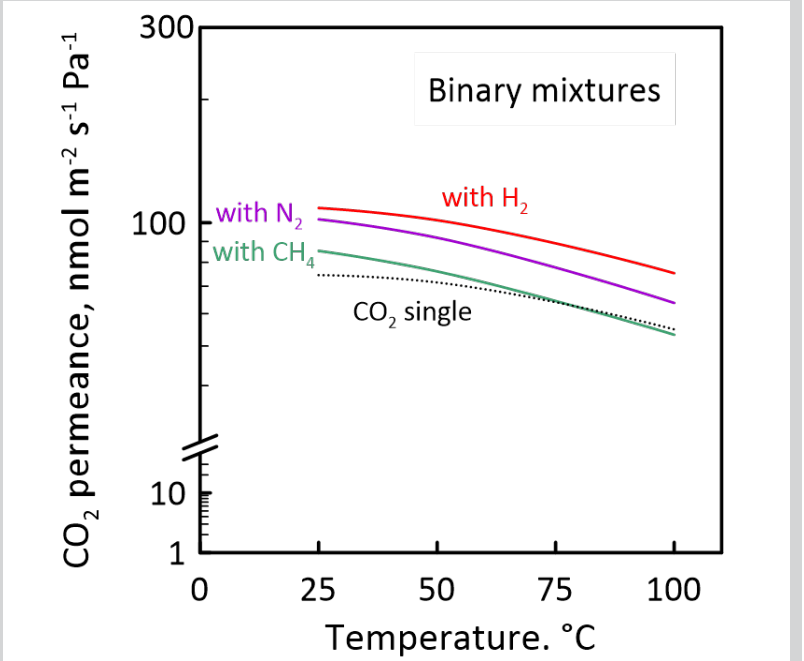

Abstract

In this work, the main aspects regarding the permeation of mixtures containing CO_2 and permanent gases such as H_2, N_2 and CH_4 through zeolite membranes have been investigated, focusing on the description of the mass transport mechanisms taking place inside the pores. First, a brief overview about the performance of the main zeolite membranes used in gas separation (e.g. DDR, CHA, AEI, FAU, etc.) was provided, which was expressed in terms of permeability and selectivity of CO_2/CH_4, CO_2/H_2 and CO_2/H_2 mixtures. The core of this work is an overview of the mass transport through the zeolite pores, with particular attention to the last achievement given by the modelling approach. Moreover, the permeation of binary mixtures has been analyzed; specifically, the effect of temperature, feed pressure and mixture composition on permeance and selectivity has been investigated. The increment of temperature and feed pressure negatively affects the separation performance of zeolite membranes, reducing both CO_2 permeance and selectivity. Moreover, the increment of CO_2 permeance observed in mixture, paired to the reduction of that of H_2, N_2 and CH_4, provides an important improvement in membrane selectivity (e.g., 6 times for CO_2/H_2 in SAPO-34). Thus, the knowledge of the appropriate operating conditions to be set, associated to the improvements in membrane reproducibility and fabrication cost, will allow to extend the applications of zeolite membranes on industrial scale.

1. Introduction

The need to face the big issue of global warming, associated to the increment in energy demand (that is expected to grow to 30% by 2040 [1]) and the depletion of fossil fuels reserves, requires concrete actions of the international community in terms of reduction of CO_2 emissions and use of greener industrial technology, based on renewable sources and Process Intensification principles. Membrane technology moves in this direction, having the potentiality to achieve better performance, lower energy consumption and volume of equipment compared to the traditional processes [2]. In gas separation, membranes can be typically divided into polymeric, inorganic and mixed matrix [3], in which inorganic materials (e.g., zeolites) are used as fillers to be incorporated in a polymeric structure. Polymeric membranes are widely used, presenting a low fabrication cost, associated to ease processing, tuneability and scalability. Nevertheless, they do not assure high chemical and thermal stability and, moreover, have important limitations related to the permeability/selectivity trade-off, as shown by the Robeson's upper bound [4]. On the contrary, inorganic membranes, which are divided

* Corresponding author: a.brunetti@itm.cnr.it (A. Brunetti)

DOI: 10.22079/JMSR.2020.124256.1366

into dense (i.e., metallic and perovskite) and porous structures (e.g., carbon, amorphous silica and zeolite), show high chemical and thermal stability, even though have a lower packing density, and in some cases their scalability is more complex than for polymer membranes. Porous inorganic membranes, as the zeolite ones, assure higher flux and chemical stability than the dense structures [3]. The major drawbacks that limited their applications in the past were the high fabrication costs and difficult in reproducibility. However, some efforts are made to reduce the fabrication costs of support, which may constitute the 70% of the total membrane cost [3]. The difficulty in scale-up of zeolite membranes for development of membrane modules, which was a big problem in the past [5], is now overcome in liquid separation as demonstrate several applications especially regarding water/alcohol pervaporation [6,7,8,9,10]. As discussed by Caro *et al.* [6] and, more recently, by Feng et al. [11], LTA membranes are applied for de-hydration of mixtures containing water and bioethanol. Also in gas separation, some attempts to scale up were carried out [12, 13]. In particular, Himeno *et al.* [12] set up a pilot plant for biogas produced in a sewage plant for CO_2:CH_4 separation using a DDR membrane. The authors obtained a CH_4 purity of 90% and 97% of CO_2, respectively, without loss of performance under operation up to 40 h. Li et al. [13] demonstrated the possibility to scaled-up a SAPO-34 membrane from 5 to 25 cm of length, maintaining the CO_2/CH_4 selectivity of the shorter membrane (about 250). However, further efforts will have to be made in reduction of fabrication cost and improvements in reproducibility to allow an ever-growing development of membranes for gas separation on industrial scale.

Zeolites represent an important class of the inorganic materials and consist of aluminosilicates with a microporous and crystalline structure. Their framework is characterized by tetrahedral building block TO_4, in which two T atoms (silicon or aluminum) are connected by oxygen in T-O-T bonds to form pores and channels [14,15]. In the zeolite structure, a SiO_4 group results neutral, whereas the AlO_4 group has a negative charge of -1. Thus, exchangeable cations (e.g., Na^+, K^+, etc.) can be located in the structure to compensate this charge. IZA, International Zeolite Association [16] classified zeolites with a three letters identification code. Based on the pore size, zeolites are distinguished into small, medium, large and ultra large structures. The Si/Al ratio, on which the adsorption capacity strongly depends, ranges from 1 (as in the case of zeolite X) to infinity (for ZSM-5 [17]). Zeolites improve their capacity to adsorb molecules when the aluminum content in its framework is higher (i.e., Si/Al is lower), since their structure become more polar [3]. Microporous character, uniform dimension of pore size, ability of ion-exchange, high thermal stability and surface area make zeolites suitable in several applications, such as adsorbent in pressure swing adsorption, catalysts for several chemical reactions, separation of liquid and gas mixtures [14]. In gas separation field, zeolites can be used in membrane shape for the separation of mixtures containing CO_2, exploiting their preferential adsorption of carbon dioxide compared to the other components that permits to achieve a high selectivity.

Here, it is discussed the possibility to use zeolite membranes for separation of CO_2 from CH_4, H_2 and N_2, which is very important in the industrial field. Specifically, removal of CO_2 from CH_4 in biogas and natural gas is necessary since CO_2 reduces their energy content, generating problems of transport and compression, also owing to its corrosive character [18]. In fact, CH_4 streams require a CO_2 concentration below 2% to be injected in the pipeline [19]. CO_2 and H_2 are the main products of syngas upgrading; their separation is needed in several processes, such as methanol and ammonia production. Finally, CO_2 and N_2 are the main components of the exhausted flue gas, whose release in the atmosphere without capturing CO_2 is the one of the main contributors to greenhouse gas emissions.

The objective of this work is to analyze the mass transport of gas mixtures through zeolite membranes, focusing on the mutual effect exerted by the strongly and weakly adsorbed species on the multicomponent permeation, as in the cases of CO_2 mixed with H_2, N_2 or CH_4. It is highlighted not only the hindering exerted by the strongly adsorbed CO_2 on the permeation of another species more weakly adsorbed, but also the positive or negative effect that such species have on the CO_2 permeation, based on the mass transport mechanisms taking place inside the pores. After a brief description of the topology of the most used zeolites and their separation performance (expressed in terms of permeance and selectivity) when used as supported membranes, the mass transport taking place through membrane pores is studied in deep, presenting the most recent achievements in the modelling analysis. Lastly, the effect of the main operating conditions (i.e., temperature, feed pressure and composition) that influence the separation performance is discussed, demonstrating the potentiality of zeolite membranes in separating CO_2-containing mixtures.

2. Permeation properties

Zeolite membranes consist of a thin zeolite layer, which is typically deposited on a porous support (as α-alumina) to obtain a membrane with high mechanical stability that can be used for separation of CO_2, light gases and hydrocarbons (Figure 1). Most of resistance to mass transport is given by the zeolite selective layer, even though porous support provides a further resistance, which depends on the pore size. This resistance may affect the separation performance of the membrane, especially when the ratio of the support permeance over the zeolite permeance is lower than 10 [3]).

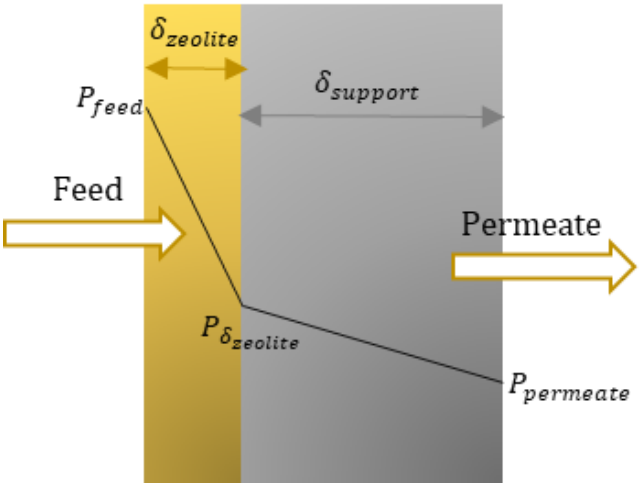

Fig. 1. Schematic view of a supported zeolite membrane.

The permeation properties of a zeolite membrane can be expressed in terms of permeance and selectivity of the components present in the feed mixture. Permeance is defined as the ratio of the permeating flux over the driving force of component *i* (Eq.1). Selectivity provides information regarding the ability of the membrane to separate one desired component from a mixture, being defined as the ratio between permeance of two components (Eq.2).

$$Permeance_i = \frac{PermeatingFlux_i}{Driving\ force_i} \quad (1)$$

$$Selectivity_{i,j} = \frac{Permeance_i}{Permeance_j} \quad (2)$$

However, permeance provides a measure of the permeation of a component through a specific membrane layer and not allow a real comparison of the separation properties among different materials, since the membrane thickness can be different. On the contrary, this comparison can be done using the permeability (Eq.3), which is a property of the material:

$$Permeability_i = Permeance_i \cdot Thickness \quad (3)$$

3. Zeolite membranes in CO_2 separation

DDR, CHA, T, MFI, FAU and AEI types are the most suitable zeolites to be used as membranes for removal of CO_2 from streams containing CH_4, N_2 and H_2. Topology of these zeolites is reported in Table 1.

The small pore Decadodecasil-3R (DDR) was one of the most investigated for the separation of carbon dioxide from methane [20, 21, 22, 23, 24, 25, 26, 27], providing the highest selectivity values (up to 500 [20,21]). DDR consists of eight-membered ring with openings that form a two-dimensional pore framework, with apertures of 3.6 Å x 4.4 Å [28].

Chabazite type (CHA), including SSZ-13 and SAPO-34, is considered one of the best candidates for separating mixtures of flue gas and natural gas [29]. CHA presents an eight-membered rings structure with a pore diameter of 3.8 Å x 3.8 Å (Figure 2 [30]). The small pore size, comparable with the dimension of several gases, associated to its strong adsorption capacity

towards CO_2, makes this material suitable for CO_2 separation from other permanent gases. In particular, Wang et al. [31] prepared high-quality SSZ-13 membranes on mullite supports and tested these membranes for CO_2/CH_4, CO_2/N_2, H_2/CH_4 and N_2/CH_4 equimolar mixtures obtaining selectivity of 406, 32, 43 and 16 at 25°C and 0.2 MPa. SAPO-34 is a silicoaluminophosphate belonging to the zeotype, consisting of SiO_4, AlO_4 and PO_4 tetrahedra. This material also provides interesting results for separation of CO_2/CH_4 [13, 32, 33, 34], CO_2/H_2 [35, 36] and CO_2/N_2 [37]. Li *et al.* [32, 37] obtained CO_2/CH_4 and CO_2/N_2 selectivity values of about 170 and 32, considering an equimolar feed stream at room temperature. In CO_2/H_2 separation, Hong *et al.* [35] measured a selectivity towards CO_2 greater than 100 at -20°C, which decreases to about 15 at 25°C. This value is similar to that measured by Mei *et al.* [36] of 17.6.

The AEI-type AIPO-18 has a three dimensional 8-membered rings framework with a diameter of 3.8 Å [28, 38]. Wang et al. [39] obtained CO_2/CH_4 and CO_2/N_2 selectivity values of 220 and 45 for equimolar mixtures.

Mordenite framework inverted (MFI) belongs to medium structures, with a 10-membered rings pore channels possesses an orthorhombic symmetry. It presents a 3-dimensional pore network, in which sinusoidal (*a*-direction) and straight channels (*b*-direction) are intersected to give a pore size of about 5.5 Å. MFI structure includes silicalite and ZSM-5, whose difference is represented by the silicon aluminium ratio, which is higher than 1000 for silicalite and ranges from 10 to infinity for ZSM-5 [40]. Silicalite was largely investigated for separation of CO_2 and permanent gases [41,42,43, 44, 45, 46, 47, 48, 49, 50, 51, 52]. Recently, Guo *et al.* [41] measured separation selectivity of 69 and 17 for CO_2/N_2 and CO_2/H_2 respectively, feeding equimolar mixtures at 20°C. Sjoberg et al. [42] tested silicalite-1 and ZSM-5 membranes prepared on graded a-alumina supports at high pressure for separation of carbon dioxide from hydrogen. The authors obtained the best performance with silicalite-1, achieving a selectivity of 48 at 273 K and 8 bar.

Zeolite T presents an intermediate framework between erionite and offretite, having a pore size of 3.6 Å x 5.1 Å and 6.7 Å x 6.8 Å [28, 53]. This material was found to be appropriate not only for water/organic liquid mixtures, but also for CO_2/CH_4 and CO_2/N_2 separation as reported by Cui *et al.* [53], who measured a CO_2/N_2 selectivity of 104 and a much higher value of 400 for CO_2/CH_4 in case of equimolar mixtures at 35°C, since CH_4 permeates slower than N_2 owing to its bigger size.

Low-silica FAU zeolites X- and Y-types (Figure 3) belong to the have a three-dimensional structure consisting of sodalite units connected by six membered double rings to give supercages. The polar structure that make them highly selective towards CO_2, which is much more adsorbed than permanent gases as H_2 and N_2 [54, 55, 56, 57, 58]. White *et al.* [55] obtained very high CO_2/N_2 selectivity (>550), which is counterbalanced by a too low CO_2 permeance value. The hydrophilic character of FAU zeolites provokes an important CO_2 permeance reduction in humid conditions. Thus, this material loses the capacity of separating CO_2 from N_2 in the moderate temperature range, whereas selectivity increases with respect to the dry condition only above 110°C [56].

However, selectivity is not the only parameter to be considered. In fact, the selection of the most appropriate membrane for a certain separation is also based on the possibility to have a high permeability. Thus, a fair compromise between selectivity and permeability is necessary, as reported in the Robeson's diagrams [4].

Table 2 summarizes selectivity and permeability of some zeolite membranes used in the literature for separation of CO_2-containing mixtures.

Table 1
Structure of several zeolite used as membranes for separation of CO_2 containing mixtures.

Structure	Material	Structure	Pore size, Å x Å
AEI	AIPO-18	8-ring	3.8 x 3.8 / 3.8 x 3.8 / 3.8 x 3.8
CHA	SAPO-34 SSZ-13	8-ring	3.8 x 3.8
DDR	DD3R	8-ring	3.6 x 4.4
ERI/OFF	T	8-ring/12-ring	6.7 x 6.8 / 3.6 x 4.9 / 3.6 x 5.1
MFI	Silicate ZSM-5	10-ring	5.1 x 5.5 / 5.3 x 5.6
FAU	NaX NaY	12-ring	7.4 x 7.4

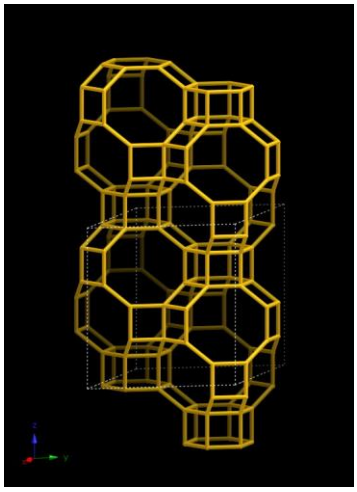

Fig. 2. Schematic view of the small pores CHA structure [30].

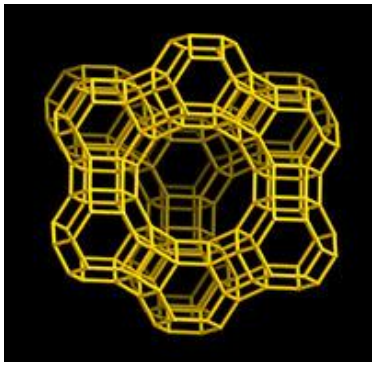

Fig. 3. Schematic view of the large pores FAU structure [30].

Table 2
Selectivity and permeability values of several zeolite used as membranes for separation of CO_2 containing mixtures.

Mixture	Material	Selectivity in the range 22-35°C	Permeability, mol m^{-1} s^{-1} Pa^{-1}	Reference
CO_2/H_2	DD3R	17	$0.14 \cdot 10^{-12}$	[27]
	SAPO-34	15	$0.19 \cdot 10^{-12}$	[35]
	NaY	28	$2.3 \cdot 10^{-12}$	[57]
CO_2/CH_4	DD3R	500	$0.23 \cdot 10^{-12}$	[20]
	DD3R	500	$0.30 \cdot 10^{-12}$	[21]
	SSZ-13	406	$2.0 \cdot 10^{-12}$	[31]
	AIPO-18	220	$5.2 \cdot 10^{-12}$	[39]
	T	400	$0.92 \cdot 10^{-12}$	[53]
	SAPO-34	170	$0.60 \cdot 10^{-12}$	[32]
CO_2/N_2	DD3R	28	$0.11 \cdot 10^{-12}$	[27]
	SSZ-13	32	$1.6 \cdot 10^{-12}$	[31]
	SAPO-34	32	$6.0 \cdot 10^{-12}$	[37]
	AIPO-18	45	$5.0 \cdot 10^{-12}$	[39]
	T	104	$0.76 \cdot 10^{-12}$	[53]
	NaY	100	$1.0 \cdot 10^{-12}$	[58]

Another important issue is that most of the industrial streams contains water vapor, which significantly reduces the permeation of the other species. When the amount of water vapor is significant, a pretreatment (e.g., a membrane condenser [59]) is necessary to remove it from the gas stream. Nevertheless, even low percentage of water vapor can drastically reduce the permeation of the gas species and modify selectivity of the membrane [20, 56, 60]. A possible solution can be to choose hydrophobic zeolite membranes to reduce the penetration of H_2O inside the pores. A DDR membrane showed a CO_2/CH_4 selectivity value of 80 at 303 K under moist conditions [20].

4. Mass transport through zeolite membranes

4.1. Single gas permeation

Permeation through zeolite layer takes place with surface diffusion at a low temperature, consisting in adsorption of the molecules onto the zeolite surface and their diffusion from site-to-site by molecular hopping [61]. The generalized Maxwell-Stefan equation was used for describing surface diffusion in zeolite pores [62, 63, 64]. In single gas conditions, the driving force for diffusion, which is represented by the potential gradient of chemical potential $\nabla\mu$, is balanced by the friction between the component and the zeolite matrix (Eq.4). For systems operating at a low pressure, chemical potential gradient can be correlated to the adsorption coverage by using the thermodynamic correction factor Γ, representing the deviation from the ideal behavior.

$$N_{SD} = -\rho C_{\mu s} D_{SD} \Gamma \nabla\theta \tag{4}$$

Specifically, $\Gamma = 1$ for the ideal condition, whereas for the non-ideal one is a function of the mixture composition [65]. In case of Langmuir adsorption model (Eq.5), thermodynamic factor is described by Eq.6 [46].

$$\theta = \frac{bP}{1+bP} \tag{5}$$

$$\Gamma = \frac{\partial \ln P}{\partial \ln \theta} = \frac{1}{1-\theta} \tag{6}$$

The Maxwell-Stefan surface diffusivity D_{SD} can depend or not on coverage. The former condition is the so-called *weak confinement scenario*, whereas the simplest dependence on coverage is the linear reduction of diffusivity (i.e., *strong confinement scenario*). However, Reed and Ehrlich [66] proposed a different expression for diffusivity, based on the intermolecular repulsions, which can reduce the energy barrier for diffusion. Considering the single gas permeation through a flat membrane, molar flux (Eq.7) can be expressed as follows in case of weak confinement scenario.

$$N_{SD} = \frac{\rho C_{\mu s} D_{SD}^0 e^{-\frac{E_{SD}}{RT}}}{\delta_{zeolite}} \ln\left(\frac{1-\theta_{\delta_{zeolite}}}{1-\theta_{feed}}\right) \tag{7}$$

However, several experimental trends of permeance as a function of temperature suggest the presence of different contribution to mass transport, especially at sufficiently high temperatures, where an adsorbed phase is not present anymore onto the inner zeolite surface, thus surface diffusion cannot describe the gas permeation. In this conditions, Xiao and Wei [67] suggested a mechanism based on permeation in the gas phase, in which molecules maintain their gaseous character passing from site-to-site by overcoming an energy barrier imposed by the presence of the channel. The so-called gas translation diffusion assumes the expression as in Eq.8 in case of negligible resistance of support.

$$N_{GTD} = \frac{1}{z}\lambda \frac{1}{\delta_{zeolite} RT} \sqrt{\frac{8RT}{\pi M}} e^{-\frac{E_{GT}}{RT}} \left(P_{feed} - P_{permeate}\right) \tag{8}$$

Several authors explained their results considering a combination between surface diffusion (at a low temperature) and gas translation diffusion (at a high temperature), whose transition is represented by a minimum in permeance [61, 68, 69, 70]. The single gas overall flux through a zeolite layer of porosity ε and tortuosity τ can be expressed, therefore, as the sum of surface and gas translation diffusion (Eq.9), supposing negligible effect of support.

$$N = \frac{\varepsilon}{\tau}\left[\frac{\rho C_{\mu s} D_{SD}^0 e^{-\frac{E_{SD}}{RT}}}{\delta_{zeolite}} \ln\left(\frac{1+bP_{feed}}{1+bP_{permeate}}\right) + \frac{\lambda}{\delta_{zeolite} RT\, z}\sqrt{\frac{8RT}{\pi M}} e^{-\frac{E_{GT}}{RT}}\left(P_{feed} - P_{permeate}\right)\right] \tag{9}$$

Other authors did not find the presence of gas translation diffusion, attributing the mass transport to surface diffusion even at a high temperature [71, 72]. They attributed the increment of flux and permeance with temperature to the presence of inter-crystalline pore openings in the membrane structure, owed to the difference in thermal expansion coefficient between support and zeolite, which can enlarge the effective pore in the polycrystalline zeolite layer, creating defects. Synthesis of membrane having a smaller crystal size (0.5 – 1 μm) should reduce this effect. Nevertheless, some experimental tests carried out on zeolite membranes having small crystals (less than 1μm) confirmed the presence of a minimum followed by an increasing trend of flux and permeance [68]. Moreover, in our opinion, the presence only of surface diffusion at a high temperature is not plausible in case of weakly adsorbed species as H_2, which present a low coverage even at moderate temperature. For these reasons, as reported in recent publications [73, 74, 75], the simultaneous presence of surface and gas translation diffusion in the whole temperature range was considered for describing the gas permeation in mixture and single gas (Figure 4). This model, which takes into-account the gas translation dependence on surface coverage as discussed in the next section, was validated for membranes of different zeolites (e.g., NaY, SAPO-34, 4A) in mixture under dry and wet conditions.

As aforementioned, a zeolite layer is deposited on a porous support to increase the mechanical stability of the membrane. The porous support can provide a further resistance to mass transport, which is associated to the Knudsen diffusion or Poiseuille flow. In a previous paper, Zito *et al.* [73] estimated the support influence on CO_2 permeation through a DD3R membrane. The authors found that an effective further resistance owed to support is present only at a low temperature (Figure 5), where the CO_2 permeance through the zeolite layer is high because of its strong adsorption, reducing the ratio between zeolite and support permeances. Differently, zeolite permeance approaches the membrane one above 400 K, since adsorption is lower and this ratio becomes very high.

4.2. Permeation in mixture

In case of a multicomponent mixture, Maxwell-Stefan equation considers the balance between the driving force attributed to the chemical potential gradient $\nabla\mu_i$ of the component *i* and its friction with the other species present in the mixture (Eq.10) [62-64, 76].

$$-\rho\theta_i \frac{\nabla\mu_i}{RT} = \sum_{j=1}^{n_{species}} \frac{C_{\mu,j} N_{SD,i} - C_{\mu,i} N_{SD,j}}{C_{\mu s,j} C_{\mu s,i} D_{SD,ij}} + \frac{N_{SD,i}}{C_{\mu s,i} D_{SD,i}} = -\rho \sum_{j=1}^{n_{species}} \Gamma_{ij} \nabla\theta_j \tag{10}$$

It can be observed the presence of the binary diffusivity $D_{SD,ij}$, representing the interaction between components *i* and *j*, which depends on the mixture composition and the single gas diffusivity. In fact, it is comprised between D_i (for $\theta_i=1$ and $\theta_j=0$) and D_j (for $\theta_i=0$ and $\theta_j=1$). The binary exchange diffusivity can be evaluated using the Vignes' correlation (Eq.11).

$$D_{SD,ij} = D_{SD,i}^{\frac{\theta_i}{\theta_i+\theta_j}} D_{SD,j}^{\frac{\theta_j}{\theta_i+\theta_j}} \tag{11}$$

An alternative expression is obtained using the self-exchange diffusivity of each component (Eq.12).

$$C_{\mu S,j} D_{SD,ij} = \left(C_{\mu S,j} D_{SD,ii}\right)^{\frac{C_{\mu,i}}{C_{\mu,i}+C_{\mu,j}}} \left(C_{\mu S,i} D_{SD,jj}\right)^{\frac{C_{\mu,j}}{C_{\mu,i}+C_{\mu,j}}} = C_{\mu S,i} D_{SD,ij} \tag{12}$$

Γ is expressed as follows (Eq.13).

$$\Gamma_{ij} = \frac{C_{\mu s,j}}{C_{\mu s,i}} \frac{C_{\mu,i}}{p_i} \frac{\partial p_i}{\partial C_{\mu,j}} \quad (13)$$

Eq.14 provides the fluxes in matrix form.

$$(N_{SD}) = \rho [C_{\mu s}] [B^{-1}] [\Gamma] (\nabla \theta) \quad (14)$$

where the elements of the matrix B are given by Eqs.15 -16.

$$B_{ii} = \frac{1}{D_{SD,i}} + \sum_{j=1}^{n_{species}} \frac{\theta_j}{D_{SD,ij}} \quad (15)$$

$$B_{ij} = -\frac{\theta_i}{D_{SD,ij}} \quad (16)$$

Gas translation diffusion flux of the generic component *ith* in the mixture has a similar expression as in single gas (Eq.8). Thus, surface and gas translation diffusion are considered to compete in permeation through the zeolite pores. Specifically, gas translation and surface diffusion of the weakly adsorbed species in mixture are hindered by the presence of an adsorbed phase and, therefore, by surface diffusion. This hindering effect is expressed in terms of a change of coverage, effective porosity and tortuosity. In particular, gas translation was considered to be dependent on surface diffusion in terms of a reduction of the effective porosity and an increment of the effective tortuosity owing to the presence of an adsorbed phase, as suggested by Caravella *et al.* [77] in presence of Knudsen coupled to surface diffusion. Afterwards, Zito *et al.* [73] demonstrated that the presence of gas translation competing with surface diffusion can describe very well the gas permeation through NaY membranes, much better than that of Knudsen. The effective porosity decreases because of the presence of an adsorbed phase, which reduces the free volume available for diffusion (Figure 6). Considering the permeation of a weakly adsorbed component as H_2 (red spheres of Figure 6), the effective porosity in single gas coincides with the nominal value of the zeolite ε_0. Differently, an increasing amount of a strong adsorbed component (blue spheres) on the active sites makes smaller this available volume. In the expression of effective porosity (Eq.17), the adsorbed molecules are assumed as spheres having a diameter equal to their kinetic diameter d_k. However, the effective volume occupied by the adsorbed molecules is considered equivalent to that of the corresponding cube, since additional volume is not accessible by the bulk molecules (i.e., between the lower part of the sphere and the zeolite surface and at the upper part of the sphere).

$$\varepsilon(C_\mu) = \varepsilon_0 - \rho(1-\varepsilon_0) N_{Av} \sum_{i=1}^{n_{species}} d_{k,i}^3 C_{\mu,i} \quad (17)$$

Differently, the effective tortuosity is increased by adsorption, since the actual path followed by the species is supposed longer than the nominal pore length owing to the presence of an adsorbed phase (Figure 6). However, when the complete surface coverage is reached, the actual path returns to the zero-loading tortuosity τ_0, since the channel assumes the same shape of the zero-loading channel again. Therefore, the effective tortuosity tends to the nominal value τ_0 in the limits of zero and complete loading of the covered surface fraction σ, which represents the surface fraction occupied by the adsorbed molecules (Eq.18).

$$\sigma(C_\mu) = \frac{\frac{\pi}{4} N_{Av} \sum_{i=1}^{n_{species}} d_{k,i}^2 C_{\mu,i}}{S_{g,0}} \quad (18)$$

In Eq.18, $S_{g,0}$ is the specific surface area at zero loading, defined as follows (Eq.19):

$$S_{g,0} = \frac{4\varepsilon_0}{\rho(1-\varepsilon_0) d_{pore,0}} \quad (19)$$

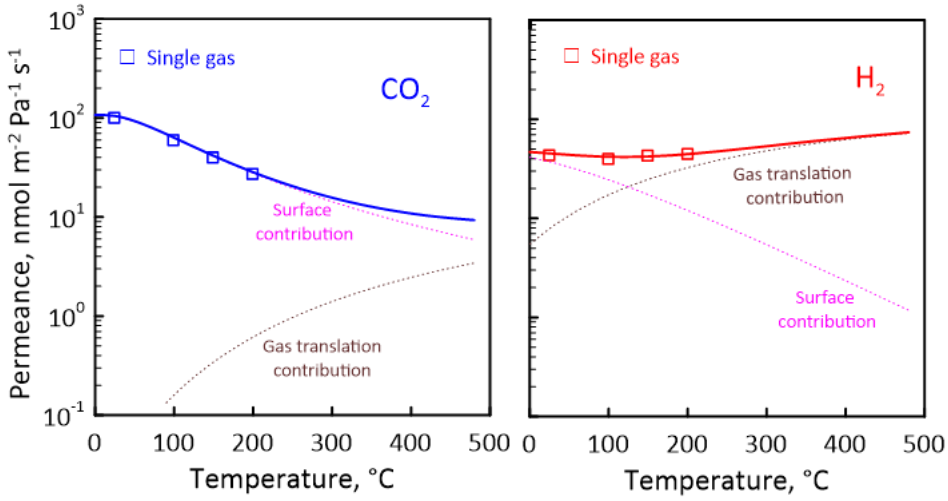

Fig. 4. Single $CO_2$and H_2 permeance as a function of temperature through a SAPO-34 membrane: experimental values (open symbol) of [68], surface diffusion contribution (magenta dotted lines), gas translation diffusion contribution (brown dotted lines) and overall permeance (solid lines). Reprinted from [74], Copyright (2020), with permission from Elsevier.

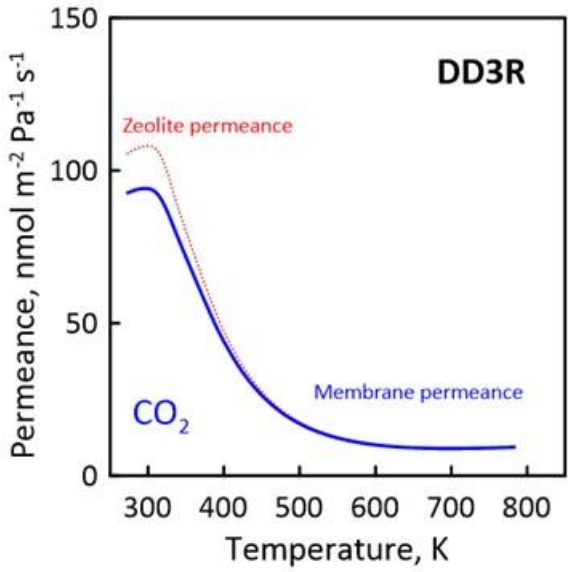

Fig. 5. CO_2 permeance through a DD3R membrane including the porous support (blue solid line) and without it (red dashed line). Reprinted from [73], Copyright (2018), with permission from Elsevier.

In addition, there is no effect of adsorption on effective tortuosity if pore size is much larger than kinetic diameter of the permeating species. In this case, effective tortuosity tends to the nominal value of the material τ_0. By defining γ as the ratio of the kinetic diameter over the pore one (Eq.20), Caravella *et al.* [77] proposed the following expression for the effective tortuosity (Eq.21).

$$\gamma = \frac{\frac{1}{n_{species}}\sum_{i=1}^{n_{species}} d_{k,i}}{d_{pore,0}} \quad (20)$$

$$\tau(C_\mu) = \tau_0 + \frac{\gamma\sigma(1-\sigma)}{\varepsilon^\gamma} \quad (21)$$

5. Discussion

5.1. Effect of temperature

Temperature significantly affects the membrane performance, modifying the behavior of both strongly and weakly adsorbed species in mixture, whose permeation is governed by surface and gas translation diffusion, respectively. Considering the strongly adsorbed species (e.g., CO_2), the increment of temperature provokes a decrease of permeance owing to the reduction of adsorption coverage as shown in case of SAPO-34 (Figure 7). CO_2 trend is quite similar to the single gas one, but a higher permeance in mixture can be observed since the reduction of its driving force in mixture is more relevant than that of permeating flux. This behavior in mixture is present in various experimental and simulation works for different zeolites and mixtures (e.g., [27, 39, 53, 68, 73,74]). However, a similar CO_2 permeance compared to the single gas condition was found in other cases (e.g., [21, 22, 58, 78]). In addition, for a fixed temperature and total feed pressure, CO_2 permeance is favored by the presence of H_2, followed by N_2 and CH_4. This phenomenon occurs because H_2 is the weakest adsorbing species among those investigated and, thus, does not compete with CO_2 in adsorption. Unlike CO_2, permeance of H_2, N_2 and CH_4 in mixture is hindered by the presence of adsorbed CO_2. Hydrogen is the most negatively affected, presenting the strong deviation from the single gas behaviour. This phenomenon is more evident at a low temperature, where CO_2 adsorption is stronger and tends to vanish when temperature increases.

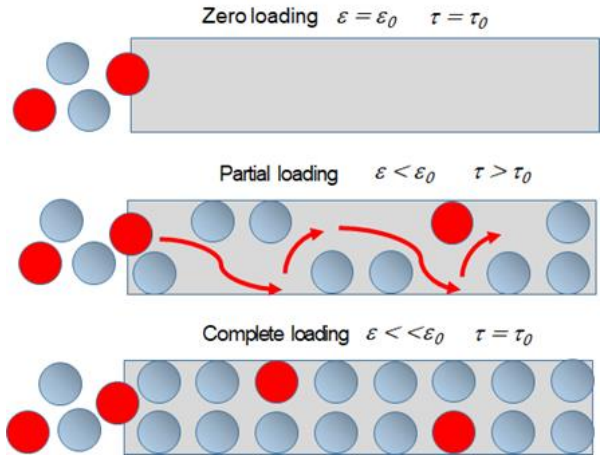

Fig. 6. Scheme of the effective porosity and tortuosity change in presence of an adsorbed phase inside the zeolite pores.

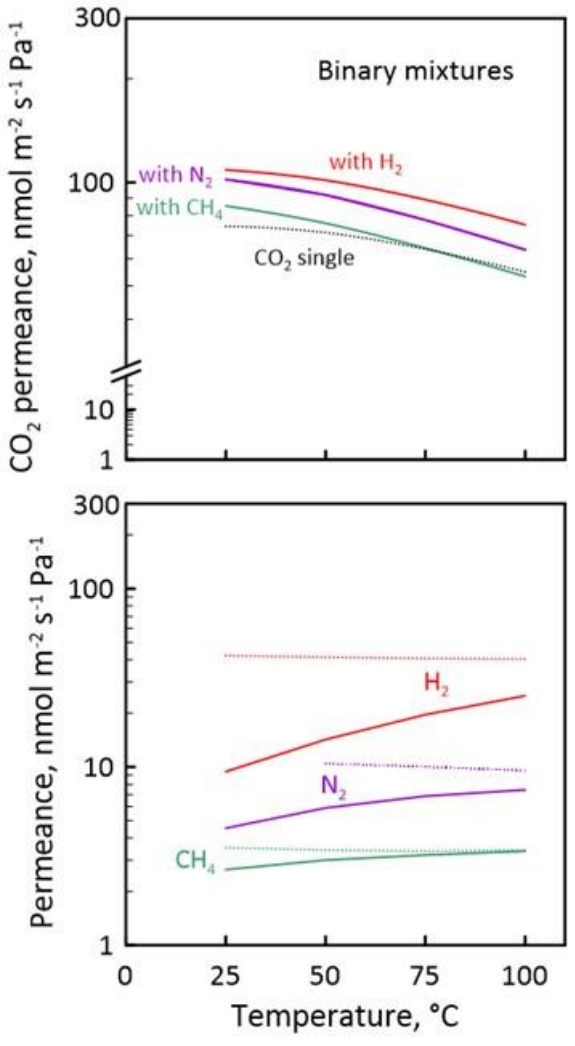

Fig. 7. CO_2,H_2 and N_2 permeance as a function of temperature for equimolar CO_2:H_2, CO_2:N_2 and CO_2:CH_4 mixtures (solid lines) and single gases (dotted lines) at a feed pressure of 500 kPa. Permeate pressure = 101 kPa. Reprinted from [74], Copyright (2020), with permission from Elsevier.

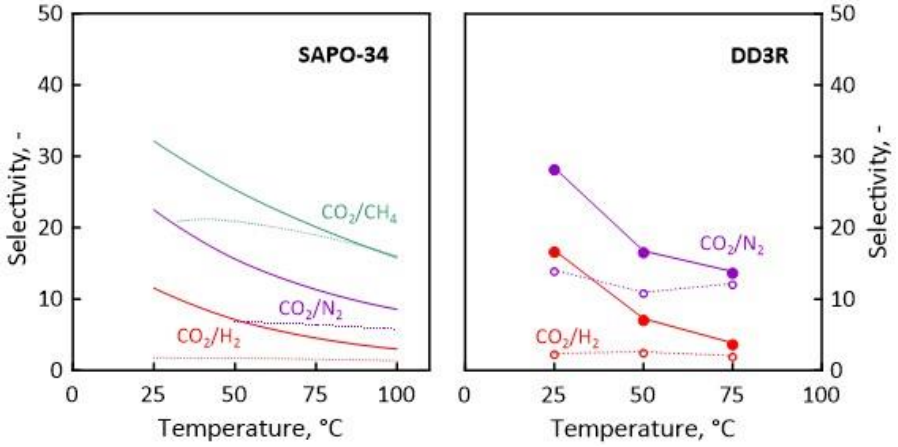

Fig. 8. Selectivity towards CO_2 as a function of temperature for binary mixtures 25°C in SAPO-45 and DD3R.Reprinted from [74], Copyright (2020), with permission from Elsevier (left side). Reprinted with permission from [27]. Copyright (2019) American Chemical Society (right side).

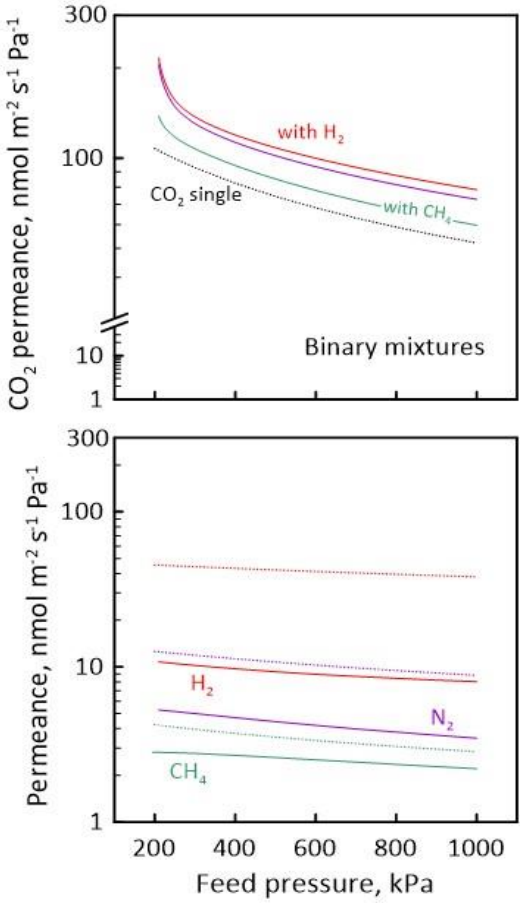

Fig. 9. CO_2, H_2 and N_2 permeance as a function of feed pressure for equimolar CO_2:H_2, CO_2:N_2 and CO_2:CH_4 mixtures (solid lines) and single gases (dotted lines) at 25°C. Permeate pressure = 101 kPa. Reprinted from [74], Copyright (2020) with permission from Elsevier.

The low temperature makes zeolite membranes very selective (Figure 8). Considering a SAPO-34 membrane, CO_2/H_2 and CO_2/N_2 selectivity values are 6 and 3 times greater in mixture at 25°C, passing from 2 to 12 and from 7 to 22, respectively [74]. The increment of temperature strongly reduces selectivity values, which approach the single gas one owing to the reduction of CO_2 adsorption. However, selectivities are much higher than the Knudsen values (i.e., 0.21, 0.80 and 0.60 for CO_2/H_2, CO_2/N_2 and CO_2/CH_4). This occurs since the quite low pore size of zeolite membranes (in general, between 0.4 and 1.2 nm), which is comparable to the dimensions of the permeating gases, causes a non-null activation energy for gaseous diffusion that takes place by gas translation instead of Knudsen.

5.2. Effect of driving force

The effect of driving force can be expressed by a variation of total feed pressure for a fixed composition or feed composition at a fixed pressure. In the former case, a negative effect of the higher feed pressure on permeance is obtained for all the components as showed in case of SAPO-34 (Figure 9), since the chemical potential gradient of the adsorbed species decreases when coverage approaches the saturation value [68]. CO_2 permeance is the most negatively affected, being the most strongly adsorbed species. Thus, selectivity is disadvantaged by the higher feed pressure. As already observed for temperature, CO_2 permeance in mixture results higher than in single gas at the same total feed pressure. The other components show a weak dependence on pressure since their diffusion partially takes place with gas translation diffusion, which is pressure-independent.

The dependence of permeance on mixture composition, which corresponds to the partial pressure of the specific component, can be expressed in terms permeance ratio, defined as the permeance of each component in mixture over that in single gas (Eq.22).

$$Permeance\ ratio_i = \frac{Permeance_i^{Mixed\ gas}}{Permeance_i^{Single\ gas}}, - \tag{22}$$

Both experimental and modelling analysis showed that CO_2 permeance decreases with increasing its composition, especially in presence of H_2, followed by N_2 and CH_4 (Figure 10). As aforementioned, this increment occurs because the reduction of driving force prevails on that of molar flux for a fixed feed pressure. Nevertheless, fixing the same CO_2 driving force, which states a higher overall feed pressure in mixture than in single gas, Zito *et al.* [74] predicted CO_2 flux and permeance in mixture much higher, similar and lower in the presence of H_2, N_2 and CH_4, respectively (Figure 11). The authors attributed this trend to the increment or reduction of the Maxwell-Stefan binary diffusivity D_{ij} (Eq.11) compared to the single CO_2 diffusivity D_i, changing its permeation in mixture (promoting or slowing effect in presence of H_2 or CH_4, respectively). In particular, the faster H_2 ($D_i = 13 \cdot 10^{-10}$ m^2 s^{-1}) encourages the CO_2 diffusion ($D_i = 1.2 \cdot 10^{-10}$ m^2 s^{-1}) in mixture increasing the binary diffusivity. On the other hand, the slower CH_4 ($D_i = 0.2 \cdot 10^{-10}$ m^2 s^{-1}) slows down CO_2 diffusion and N_2 ($D_i = 1.8 \cdot 10^{-10}$ m^2 s^{-1}) has slight influence on D_{ij}. Unlike carbon dioxide, H_2, N_2 and CH_4 in mixture show a permeance lower than in single gas and reduced by the increasing CO_2 composition owing to the most important hindering effect.

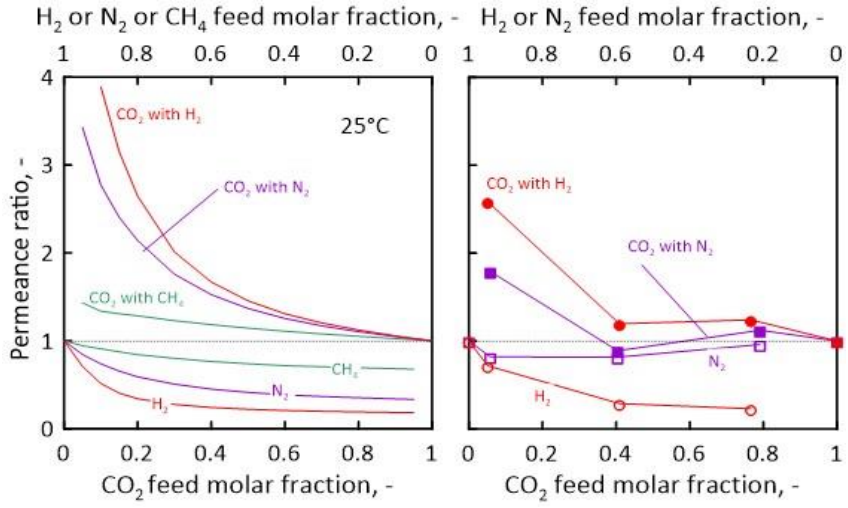

Fig. 10. CO_2, CH_4, N_2 and H_2 permeance ratios as a function of CO_2 feed molar fraction for binary mixtures at a feed pressure of 500 kPa and 25°C.Reprinted from [74], Copyright (2020), with permission from Elsevier (left side). Adapted with permission from [27]. Copyright (2019) American Chemical Society (right side).

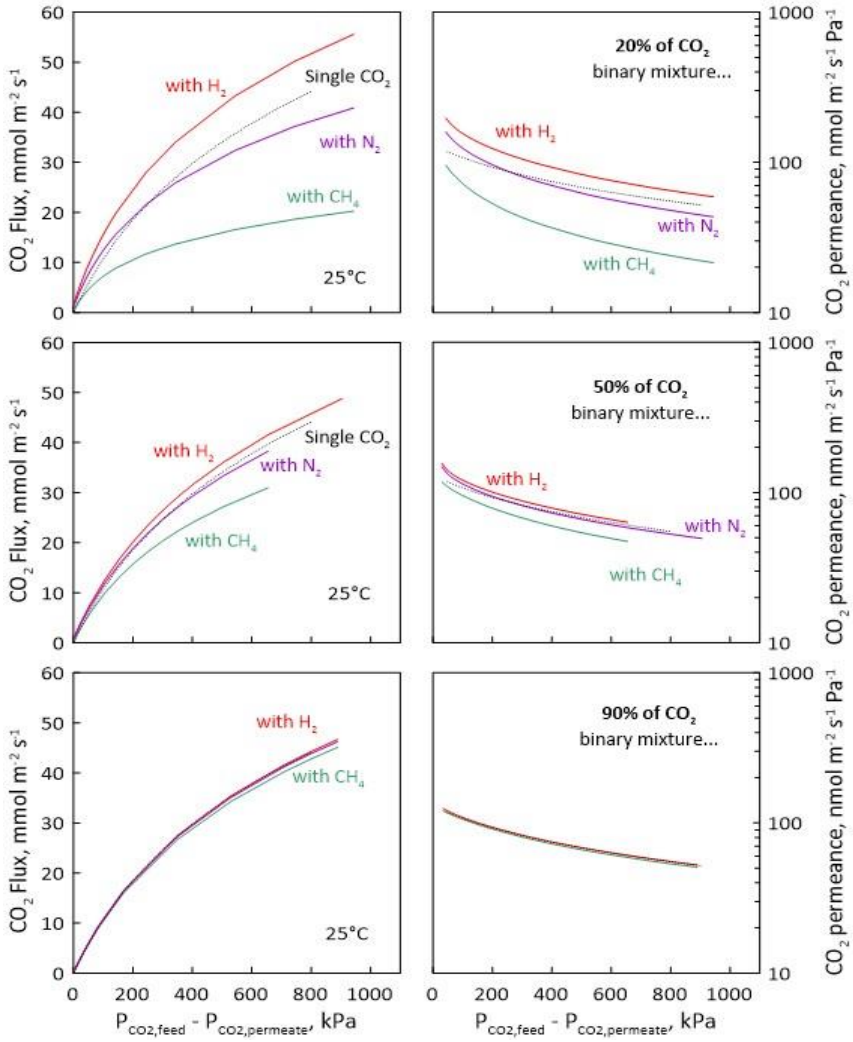

Fig. 11. CO_2 molar flux and permeance as a function of CO_2 driving force for mixtures (solid lines) and single gas (dotted line).Reprinted from [74], Copyright (2020), with permission from Elsevier.

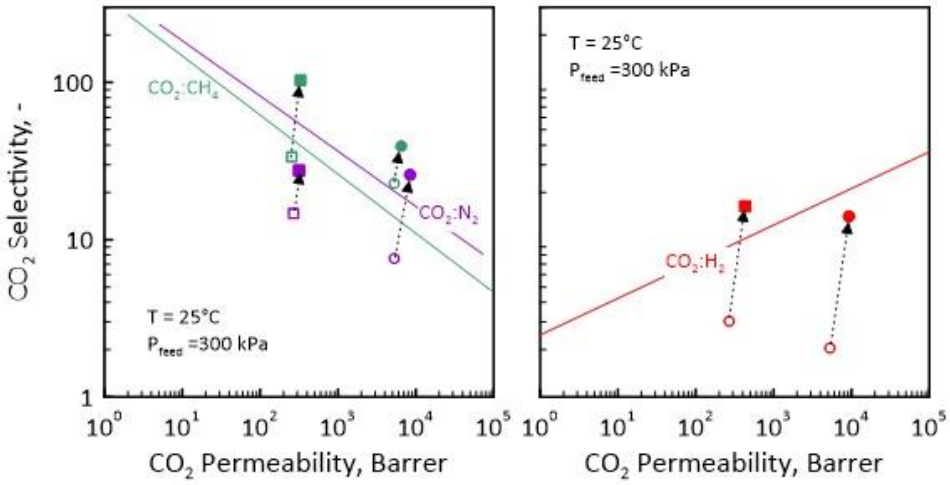

Fig. 12. CO_2/N_2, CO_2/CH_4 and CO_2/H_2 selectivity as a function of CO_2 permeability through DD3R (squares) and SAPO-34 (circles) in binary mixture (full symbols) and single gas (open symbols). Upper bounds [4,79] (solid lines).

The selectivity versus permeability values in single gas and mixtures can be better appreciated using the upper bounds [4,79] for different pairs of gases. The single gas condition (open symbols of Figure 12) is characterized by lower CO_2 permeability and selectivity, thus, a minor possibility to overcome the upper bound at room temperature. On the contrary, a significant increment of selectivity towards carbon dioxide can be achieved in mixture, since the strong CO_2 adsorption hinders the diffusion of the other component. Moreover, a higher CO_2 permeability in mixture can be observed, as revealed by the positive slope of each line connecting single gas and mixture values, favoring the possibility to exceed the upper bound.

6. Conclusions

Zeolite membranes can successfully separate CO_2 from mixtures containing CH_4, H_2 and N_2 because of CO_2 preferential adsorption that favors its permeation and hinders that of the other species weaker adsorbed. An analysis of the state-of-the-art revealed that CO_2 can be more selectively removed from H_2 and N_2 using NaY membranes, which allow very high selectivity at room temperature owing to the NaY polar structure that favors the strong CO_2 adsorption with respect to the permanent gases. Differently, CO_2/CH_4 mixtures can be better separated using small or intermediate pore structures (i.e., DDR, AIPO-18, SAPO-34 and T), exploiting the pore size comparable to the CH_4 dimension, which slows down its diffusion.

Mass transport of mixtures through zeolite membranes can be successfully described using a model considering the simultaneous presence of surface and gas translation diffusion, which are considered to be in competition. In particular, the presence of a strongly adsorbed component (e.g., CO_2) not only impedes the possibility to another component to be adsorbed, but also reduces the volume available to its diffusion (i.e., effective porosity) and increase the real path to be followed in the gas phase (i.e., effective tortuosity), impeding the free gas translation contribution to mass transport. Thus, permeance and selectivity highly vary passing from single gas to mixture conditions. Moreover, the mutual influence between the permeating components on the binary diffusivity encouraged CO_2 permeation in presence of H_2, whereas slowed it in presence of CH_4. Lastly, N_2 does not significantly affect CO_2 permeation, having a diffusivity similar to carbon dioxide. The combined effect of adsorption and diffusion makes selectivity in mixture improved with respect to the single gas value. Increments of temperature, feed pressure and CO_2 composition have a negative effect on CO_2 permeance and, in addition, reduce the membrane selectivity. The knowledge of permeance and selectivity and their dependence on the operating conditions is a first important step in the design of a separation unit.

Acknowledgments

The project BIOVALUE "Advanced Membranes for biogas upgrading and high added value compounds recovery", co-funded by Regione Calabria in the framework of M-Era.Net 2018 is gratefully acknowledged.

Notation

B	Inverted diffusivity matrix in the Maxwell-Stefan model, s m^{-2}
B_{ii}	Element of matrix [B], defined by Eq.15, s m^{-2}
B_{ij}	Element of matrix [B], defined by Eq.16, s m^{-2}
b	Langmuir's affinity constant, Pa^{-1}
C_μ	Molecular loading, mol·kg^{-1}
$C_{\mu s}$	Saturation molecular loading, mol·kg^{-1}
$C_{\mu s0}$	Saturation loading of component *i* at the reference temperature, mol·kg^{-1}
D^0_{SD}	Pre-exponential factor for surface diffusivity, m^2 s^{-1}
D_{SD}	Surface self-diffusivity, m^2 s^{-1}
$D_{SD,ii}$	Self-exchange diffusivity of component *i* , m^2 s^{-1}
$D_{SD,ij}$	Binary diffusivity of surface diffusion, m^2 s^{-1}
$D_{SD,jj}$	Self-exchange diffusivity of component *j*, m^2 s^{-1}
d_k	Kinetic diameter of the molecules, m
$d_{pore,0}$	Mean pore diameter at zero-loading conditions, m
E_{GT}	Activation energy for gas translation diffusion, J mol^{-1}
E_{SD}	Activation energy for surface diffusion, J mol^{-1}
M	Molar mass, kg mol^{-1}
N	Molar flux, mol s^{-1} m^{-2}
N_{Av}	Avogadro's number, mol^{-1}
P	Pressure, Pa
R	Gas constant, 8.314 J·mol^{-1}·K^{-1}
$S_{g,0}$	Zero-loading specific area, m^2 kg^{-1}
T	Temperature, K
T_0	Reference temperature, K
z	Coordination number, -
Greek letters	
Γ	Thermodynamic factor, -
γ	Parameter described by Eq.20, -
∇	Gradient operator, m^{-1}
δ	Membrane thickness, m
$\delta_{zeolite}$	Zeolite layer thickness, m
ε_0	Porosity at zero-loading conditions, -
ε	Effective porosity, -
λ	Diffusional length, m
μ	Chemical potential, J mol^{-1}
θ	Loading degree, -
ρ	Zeolite density, kg m^{-3}
σ	Covered surface fraction, -
τ_0	Tortuosity at zero-loading conditions, -
τ	Effective tortuosity, -
Subscripts / Superscripts	
i,*j*	Generic *i-th* and *j-th* species

References

[1] A.H. Alami, A.A. Hawili, M. Tawalbeh, R. Hasan, L. Al Mahmoud, S. Chibib, A. Mahmood, K. Aokal, P. Rattanapanya, Materials and logistics for carbon dioxide capture, storage and utilization, Sci. Total Environ. 717 (2020) 137221.

[2] E. Drioli, A. Brunetti, G. Di Profio, G. Barbieri, Process Intensification strategies and membrane engineering, Green Chem. 14 (2012) 1561-1572.

[3] N. Kosinov, J. Gascon, F. Kapteijn, E.J.M. Hensen, Recent developments in zeolite membranes for gas separation, J. Membr. Sci. 499 (2016) 65-79.

[4] L.M. Robeson, The upper bound revisited, J. Membr. Sci. 320 (2008) 390-400.

[5] J. Caro, M. Noack, P. Kolsch, R. Schafer, Zeolite membranes – state of their development and perspective, Micropor. Mesopor. Mater. 38 (2000) 3-24.

[6] J. Caro, M. Noack, Zeolite membranes – Recent developments and progress, Micropor. Mesopor. Mater. 115 (2008) 215-233.

[7] Y. Morigami, M. Kondo, J. Abe, H. Kita, K. Okamoto, The first large-scale pervaporation plant using tubular-type module with zeolite NaA membrane, Sep. Purif. Technol. 25 (2001) 251-260.

[8] T. Gui, F. Zhang, Y. Li, X. Cui, X. Wu, M. Zhu, N. Hu, X. Chen, H. Kita, M. Kondo, Scale-up of NaA zeolite membranes using reusable stainless steel tubes for dehydration in an industrial plant, J. Membr. Sci. 583 (2019) 180-189.

[9] M. Ji, X. Gao, X. Wang, Y. Zhang, J. Jiang, X. Gu, An ensemble synthesis strategy for fabrication of hollow fiber T-type zeolite membrane modules, J. Membr. Sci. 563 (2018) 460-469.

[10] A. Garofalo, M.C. Carnevale, L. Donato, E. Drioli, O. Alharbi, S.A. Aljlil, A. Criscuoli, C. Algieri, Scale-up of MFI membranes for desalination by vacuum membrane distillation, Desalination 397 (2016) 205-212.

[11] C. Feng, K.C. Khulbe, T. Matsuura, R. Farnood, A.F. Ismail, Recent progress in zeolite/zeotype membranes, J. Membr. Sci. Res. 1 (2015) 49-72.

[12] S. Himeno , K. Takeya, S. Fujita, Development of biogas separation process using DDR-type zeolite membrane, Kagaku kōgaku ronbunshū 36 (2010) 545-551.

[13] S. Li, M.A. Carreon, Y. Zhang, H.H. Funke, R.D. Noble, J.L. Falconer, Scale-up of SAPO-34 membranes for CO_2/CH_4 separation, J. Membr. Sci. 352 (2010) 7-13.

[14] A. Tavolaro, E. Drioli, Zeolite membranes, Adv. Mater. 11 (1999) 975-996.

[15] K.S. Walton, M.B. Abney, M.D. LeVan, CO_2 adsorption in Y and X zeolites modified by alkali metal cation exchange, Micropor. Mesopor. Mater. 91 (2006) 78-84.

[16] http://www.iza-online.org/

[17] K. Makrodimitris, G.K. Papadopoulos, D.N. Theodorou, Prediction of permeation properties of CO_2 and N_2 through silicalite via molecular simulations, J. Phys. Chem. B 105 (2001) 777-788.

[18] S. Basu, A.L. Khan, A. Cano-Odena, C. Liu, I.F.J. Vankelecom, Membrane-based technologies for biogas separations, Chem. Soc. Rev. 39 (2010) 750-768.

[19] R.W. Baker, Future directions of membrane gas separation technology, Ind. Eng. Chem. Res. 41 (2002) 1393-1411.

[20] L. Wang, C. Zhang, X. Gao, L. Peng, J. Jiang, X. Gu, Preparation of defect-free DDR zeolite membranes by eliminating template with ozone at low temperature, J. Membr. Sci. 539 (2017) 152-160.

[21] J. van den Bergh, W. Zhu, J. Gascon, J.A. Moulijn, F. Kapteijn, Separation and permeation characteristics of a DD3R zeolite membrane, J. Membr. Sci. 316 (2008) 35-45.

[22] T. Tomita, K. Nakayama, H. Sakai, Gas separation characteristics of DDR type zeolite membrane, Micropor. Mesopor. Mater. 68 (2004) 71-75.

[23] S. Yang, Z. Cao, A. Arvanitis, X. Sun, Z. Xu, J. Dong, DDR-type zeolite membrane synthesis, modification and gas permeation studies, J. Membr. Sci. 505 (2016) 194-204.

[24] S. Himeno, T. Tomita, K. Suzuki, K. Nakayama, K. Yajima, S. Yoshida, Synthesis and permeation properties of a DDR-type zeolite membrane for separation of CO_2/CH_4 gaseous mixtures, Ind. Eng. Chem. Res. 46 (2007) 6989-6997.

[25] H. Hasegawa, K. Nishida, S. Oguro, Y. Fujimura, K. Yajima, M. Niino, M. Isomura, T. Tomita, Gas separation process for CO_2 removal from natural gas with DDR-type zeolite membrane, Energy Procedia 114 (2017) 32-36.

[26] M.J. Vaezi, A.A. Babaluo, H. Maghsoudi, Synthesis, modification and gas permeation properties of DD3R zeolite membrane for separation of natural gas impurities (N_2 and CO_2), J. Nat. Gas Sci. Eng. 52 (2018) 423-431.

[27] P.F. Zito, A. Brunetti, E. Drioli, G. Barbieri, CO_2 separation via a DDR membrane: mutual influence of mixed gas permeation, Ind. Eng. Chem. Res. 59 (2020) 7054-7060

[28] Ch. Baerlocher, L.B. McCusker, D.H. Olson, Atlas of zeolite framework types, Sixth revised Edition, Elsevier, Amsterdam, 2007.

[29] B. Liu, C. Tang, X. Li, B. Wang, R. Zhou, High-performance SAPO-34 membranes for CO_2 separations from simulated flue gas, Micropor. Mesopor. Mater. 292 (2020) 109712.

[30] Ch. Baerlocher and L.B. McCusker, Database of Zeolite Structures: http://www.iza-structure.org/databases/

[31] B. Wang, Y. Zheng, J. Zhang, W. Zhang, F. Zhang, W. Xing, R. Zhou, Separation of light gases using zeolite SSZ-13 membranes, Micropor. Mesopor. Mater. 275 (2019) 191-199.

[32] S. Li, J.L. Falconer, R.D. Noble, SAPO-34 membranes for CO_2/CH_4 separations: effect of Si/Al ratio, Micropor. Mesopor. Mater. 110 (2008) 310-317.

[33] Y. Chen, Y. Zhang, C. Zhang, J. Jiang, X. Gu, Fabrication of high-flux SAPO-34 membrane on α-Al_2O_3 four-channel hollow fibers for CO_2 capture from CH_4, J. CO_2 Utilization 18 (2017) 30-40.

[34] J.C. Poshusta, V.A. Tuan, E.A. Pape, R.D. Noble, J.L. Falconer, Separation of light gases using SAPO-34 membranes, AIChE J. 46 (2000) 779-789.

[35] M. Hong, S. Li, J.L. Falconer, R.D. Noble, Hydrogen purification using a SAPO-34 membrane, J. Membr. Sci. 307 (2008) 277-283.

[36] W. Mei, Y. Du, T. Wu, F. Gao, B. Wang, J. Duan, J. Zhou, R. Zhou, High-flux CHA zeolite membranes for H_2 separations, J. Membr. Sci. 565 (2018) 358-369.

[37] S. Li, C.Q. Fan, High-flux SAPO-34 membrane for CO_2/N_2 separation, Ind. Eng. Chem. Res. 49 (2010) 4399-4404.

[38] T. Wu, B. Wang, Z. Lu, R. Zhou, X. Chen, Alumina-supported AIPO-18 membranes for CO_2/CH_4 separation, J. Membr. Sci. 471 (2014) 338-346.

[39] B. Wang, N. Hu, H. Wang, Y. Zheng, R. Zhou, Improved AIPO-18 membranes for light gas separation, J. Mater. Chem. A 3 (2015) 12205.

[40] K. Makrodimitris, G.K. Papadopoulos, D.N. Theodorou, Prediction of Permeation Properties of CO_2 and N_2 through Silicalite via Molecular Simulations, J. Phys. Chem. B 105 (2001) 777-788.

[41] H. Guo, G. Zhu, H. Li, Z. Zou, X. Yin, W. Yang, S. Qiu, R. Xu, Hierarchical growth of large-scale ordered zeolite silicalite-1 membranes with high permeability and selectivity for recycling CO_2, Angew. Chem. 118 (2006) 7211-7214.

[42] E. Sjöberg, S. Barnes, D. Korelskiy, J. Hedlund, MFI membranes for separation of carbon dioxide from synthesis gas at high pressure, J. Membr. Sci. 486 (2015) 132-137.

[43] S.K. Wirawan, D. Creaser, J. Lindmark, J. Hedlund, I.M. Bendiycasa, W.B. Sediawan, H_2/CO_2 permeation through a silicalite-1 composite membrane, J. Membr. Sci. 375 (2011) 313-322.

[44] L.J.P. van den Broeke, W.J.W. Bakker, F. Kapteijn, J.A. Moulijn, Binary Permeation through a Silicalite-1 Membrane, AIChE J. 45 (1999) 976-985.

[45] J.C. Poshusta, R. D. Noble, J.L. Falconer, Temperature and pressure effects on CO_2 and CH_4 permeation through MFI zeolite membranes, J. Membr. Sci. 160 (1999) 115-125.

[46] W.J.W. Bakker, F. Kapteijn, J. Poppe, J.A. Moulijn, Permeation characteristics of a metal-supported silicalite-1 zeolite membrane, J. Membr. Sci. 117 (1996) 57-78.

[47] W. Zhu, P. Hrabanek, L. Gora, F. Kapteijn, J.A. Moulijn, Role of Adsorption in the Permeation of CH_4 and CO_2through a Silicalite-1 Membrane, Ind. Eng. Chem. Res. 45 (2006) 767-776.

[48] M.C. Lovallo, A. Gouzinis, M. Tsapatsis, Synthesis and Characterization of Oriented MFI Membranes Prepared by Secondary Growth, AIChE J. 44 (1998) 1903-1913.

[49] H. Wang, Y.S. Lin, Effects of Water Vapor on Gas Permeation and Separation Properties of MFI Zeolite Membranes at High Temperatures, AIChE J. 58 (2012) 153-162.

[50] F. Akhtar, E. Sjöberg, D. Korelskiy, M. Rayson, J. Hedlund, L. Bergström, Preparation of graded silicalite-1substrates for all-zeolite membranes with excellent CO_2/H_2 separation performance, J. Membr. Sci. 493 (2015) 206-211.

[51] M. Tawalbeh, F.H. Tezel, M- Al-Ismaily, B. Kruczek, Highly permeable tubular silicalite-1 membranes for CO_2 capture, Sci. Total Environ. 676 (2019) 305-320.

[52] M. Tawalbeh, F.H. Tezel, S. Letaief, C. Detellier, B. Kruczek, Separation of CO_2 and N_2 on zeolite silicalate-1 membrane synthesized on novel support, Sep. Sci. Technol. 47 (2012), 1606-1616.

[53] Y. Cui, H. Kita, K. Okamoto, Preparation and gas separation performance of zeolite T membrane, J. Mater. Chem. 14 (2004) 924-932.

[54] B.-H. Jeong, Y. Hasegawa, K.-I. Sotowa, K. Kusakabe, S. Morooka, Permeation of binary mixtures of benzene and saturated C4-C7 hydrocarbons through an FAU-type zeolite membrane, J. Membr. Sci. 213 (2003) 115-124.

[55] JC. White, P.K. Dutta, K. Shqau, H. Verweij, Synthesis of ultrathin zeolite Y membranes and their application for separation of carbon dioxide and nitrogen gases, Langmuir 26 (2010) 10287-10293.

[56] X. Gu, J. Dong, T.M. Nenoff, Synthesis of defect-free FAU-type zeolite membranes and separation for dry and moist CO_2/N_2 mixtures, Ind. Eng. Chem. Res. 44 (2005) 937-944.

[57] K. Kusakabe, T. Kuroda, K. Uchino, Y. Hasegawa, S. Morooka, Gas permeation properties of ion-exchanged faujiasite-type zeolite membranes, AIChE J. 45 (1999) 1220-1226.

[58] K. Kusakabe, T. Kuroda, A. Murata, S. Morooka, Formation of a Y-type zeolite membrane on a porous a-alumina tube for gas separation, Ind. Eng. Chem. Res. 36 (1997) 649-655.

[59] A. Brunetti, F. Macedonio, G. Barbieri, E. Drioli, Membrane condenser as emerging technology for water recovery and environment protection: perspectives and potentialities, BMC Chemical Engineering- Springer Nature, (2019), 1-19. DOI: 10.1186/s42480-019-0020-x

[60] W. Zhu, L. Gora, A.W.C. van den Berg, F. Kapteijn, J.C. Jansen, J.A. Moulijn, Water vapour separation from permanent gases by a zeolite-4A membrane, J. Membr. Sci. 253 (2005) 57-66.

[61] W.J.W. Bakker, L.J.P. van den Broeke, F. Kapteijn, J.A. Moulijn, Temperature dependence of one-component permeation through a silicalite-1 membrane, AIChE J. 43 (1997) 2203-2214.

[62] R. Krishna, Multicomponent surface diffusion of adsorbed species. A description based on the generalized Maxwell-Stefan diffusion equations, Chem. Eng. Sci. 45 (1990) 1779-1791.

[63] R. Krishna, A unified approach to the modelling of intraparticle diffusion in adsorption processes, Gas Separ. Purif. 7 (1993) 91-104.

[64] R. Krishna, Problems of pitfalls in the use of the Fick formulation for intraparticle diffusion, Chem. Eng. Sci. 48 (1993) 845-861.

[65] R. Krishna, , J.A. Wesselingh, The Maxwell-Stefan approach to mass transfer, Chem. Eng. Sci. 52 (1997) 861-911.

[66] D.A. Reed, G. Ehrlich, Surface diffusion, atomic jump rates and thermodynamics, Surf. Sci. 102 (1981) 588-609.

[67] J. Xiao, J. Wei. Diffusion mechanism of hydrocarbons in zeolites – I. Theory, Chem. Eng. Sci. 47 (1992) 1123-1141.

[68] S. Li, J.L Falconer, R.D. Noble, SAPO-34 membranes for CO_2/CH_4 separation, J. Membr. Sci. 241 (2004) 121-135.

[69] J.C. Poshusta, V.A. Tuan, J.L. Falconer, R.D. Noble, Synthesis and permeation properties of SAPO-34 tubular membranes, Ind. Eng. Chem. Res. 37 (1998) 3924-3929.

[70] T. Wu, B. Wang, Z. Lu, R. Zhou, X. Chen, Alumina-supported AIPO-18 membranes for CO_2/CH_4 separation, J. Membr. Sci. 471 (2014) 338-346.

[71] S. Miachon, P. Ciavarella, L. van Dyk, I. Kumakiri, K. Fiaty, Y. Schuurman, J.-A. Dalmon, Nanocomposite MFI-alumina membranes via pore-plugging synthesis: Specific transport and separation properties, J. Membr. Sci. 298 (2007) 71-79.

[72] J. van den Bergh, A. Tihaya, F. Kapteijn, High temperature permeation and separation characteristics of an all-silica DDR zeolite membranes, Micropor. Mesopor. Mater. 132 (2010) 137-147.

[73] P.F. Zito, A. Caravella, A. Brunetti, E. Drioli, G. Barbieri, Discrimination among gas translation, surface and Knudsen diffusion in permeation through zeolite membranes, J. Membr. Sci. 564 (2018) 166-173.

[74] P.F. Zito, A. Brunetti, A. Caravella, E. Drioli, G. Barbieri. Mutual influence in permeation of CO_2-containing mixtures through a SAPO-34 membrane, J. Membr. Sci. 595 (2020) 117534.

[75] P.F. Zito, A. Brunetti, A. Caravella, E. Drioli, G. Barbieri. Water vapor permeation and its influence on gases through a zeolite-4A membrane, J. Membr. Sci. 574 (2019) 154-163.

[76] F. Kapteijn, J.A. Moulijn, R. Krishna, The generalized Maxwell-Stefan model for diffusion in zeolites: sorbate molecules with different saturation loadings, Chem. Eng. Sci. 55 (2000) 2923-2930.

[77] A. Caravella, P.F. Zito, A. Brunetti, E. Drioli, G. Barbieri, A novel modelling approach to surface and Knudsen multicomponent diffusion through NaY zeolite membranes, Micropor. Mesopor. Mater. 235 (2016) 87-99.

[78] Y. Hasegawa, K. Kusakabe, S. Morooka, Effect of temperature on the gas permeation properties of NaY-type zeolite formed on the inner surface of a porous support tube, Chem. Eng. Sci. 56 (2001) 4273-4281.

[79] H.Q. Lin, E. Van Wagner, B.D. Freeman, L.G. Toy, R.P. Gupta, Plasticization-enhanced hydrogen purification using polymeric membranes, Science 311 (2006) 639.